Structures and Phases in (Nano-) Systems in Confined Geometry

M. Beck, B. Gast, S. Haun, M. Matt, F. Müller, M. Pütz, M. Ring, R. W. U. Schmid, U. Siems, U. Steinwandel, T. Vater, P. Nielaba

published in

NIC Symposium 2018
K. Binder, M. Müller, A. Trautmann (Editors)

Forschungszentrum Jülich GmbH,
John von Neumann Institute for Computing (NIC),
Schriften des Forschungszentrums Jülich, NIC Series, Vol. 49,
ISBN 978-3-95806-285-6, pp. 75.
http://hdl.handle.net/2128/17544

Structures and Phases in (Nano-) Systems in Confined Geometry

Marcus Beck, Bastian Gast, Steffen Haun, Manuel Matt, Fabian Müller, Martin Pütz, Markus Ring, Ralf W. U. Schmid, Ullrich Siems, Ulrich Steinwandel, Tobias Vater, and Peter Nielaba

Department of Physics, University of Konstanz, 78457 Konstanz, Germany
E-mail: {marcus.beck, bastian.gast, steffen.haun, manuel.matt, fabian.3.mueller, martin.puetz, markus.ring, ralf.schmid, ullrich.siems, ulrich.steinwandel, tobias.vater, peter.nielaba}@uni-konstanz.de

Computer simulations by members of the NIC-project HMZ07 are reviewed. Structural and transport properties have been investigated in atomic wires by Molecular Dynamics and electronic transport methods and in model colloids by Brownian Dynamics. Spinodal decomposition and domain growth of liquid-vapour systems and galaxy magnetism have been studied by hydrodynamics simulations, and nucleation phenomena in lattice systems by rare event methods.

1 Introduction

In our NIC-project HMZ07, computer simulations of many body systems have been done. The systems we investigated (colloids, nano wires, fluids, crystallites) and the scientific questions (structure formation, transport, phase transitions) are of relevance for the SFBs 767 and 1214 at the University of Konstanz. Here we review and present recent results obtained in our NIC project.

In Sec. 2, we report on the computations of electronic and structural properties of atomic wires. In Sec. 3, the effects of external periodic light fields and driving forces on the structural and dynamical properties of two dimensional colloidal systems, confined in a channel geometry, are analysed by Brownian Dynamics simulations as well as the effect of counterflow on segregation phenomena and the ordering on non-spherical particles in channel geometry. In Sec. 4, results for nucleation phenomena in lattice systems, obtained by rare event methods, are presented, and in Sec. 5, results of hydrodynamics simulations for spinodal decomposition phenomena.

2 Conductance of Atomic Sized Contacts

The potential to construct electronic devices with functional building blocks of atomic size is a major driving force of nanotechnology. In cooperation with experimental groups world wide we study the structural and electronic properties of atomic wires.

In the last years the trend towards smaller and more powerful electronic devices continued, which we find in modern smartphones and laptops, but which are as well of great importance for scientific investigations with supercomputers. In this context the question arises, down to which smallest length sizes one can still speak of wires, which contact

electronic devices, and which physical phenomena become relevant. Of course, on smallest length scales quantum mechanics will become important, which is not considered in classical considerations. Beyond this, the question arises, what the smallest cross section is for smallest wires. A wire with a linear structure of atoms is here the answer. The most important example is an atomic wire consisting of Au atoms[1], besides an other example of (short) Pt wires. These materials form during a process of a continuing stretching in wire direction "atomic nano wires". The phenomena during the formation of such atomic wires in such materials can be traced back to the fact that the atomic bonds between two neighbour atoms are energetically more favourable in a linear order compared to a regular order in a solid, due to relativistic effects.

Metals, which transport electrical current very well, usually also transport heat very well. In both transport processes, the energy is mainly transported by the same particles, free electrons. The application of a voltage at the ends of a metallic wire results in an electrical current, a charge transport. By this process, the wire not only heats up, but with the charge carrier motion an energy or heat transport is linked, a "heat current". The relation between the charge transport and the heat transport in metals can be described by the empirical Wiedemann-Franz law. The transport phenomena are described by the quantities "heat conductance" κ and "charge conductance" G, and the Wiedemann-Franz law states -independent of the specific metal- , that $\kappa = L_0 T G$, where T is the temperature, and L_0 the Lorenz-number, which can be computed in a classical Drude-Sommerfeld model as $L_0 = \pi^2 k_B^2/(3e^2)$, with the Boltzmann constant k_B and the elementary charge e.

Atomic wires are excellent systems to analyse the electrical transport as well as the heat transport on atomic length scales. An experimental investigation of these phenomena is demanding and became possible only recently[2] (in the experimental groups of E. Meyhofer and P. Reddy, U. Michigan (USA)), for which our theoretical modelling has been very

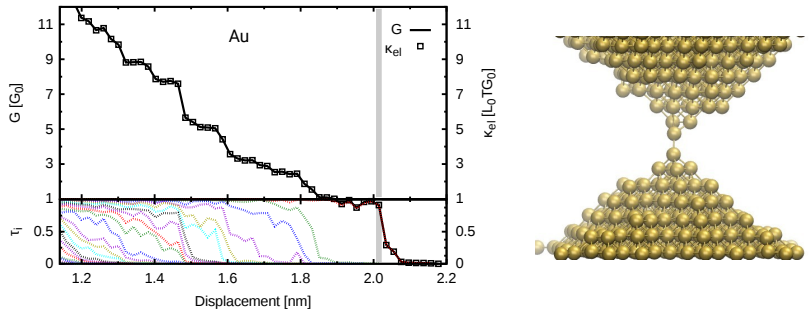

Figure 1. Electric conductance G and thermal conductance κ for atomic Au-contacts as function of the electrode distance, $G_0 = 2e^2/h$, $L_0 = \pi^2 k_B^2/(3e^2)$.[2] The coloured lines in the lower part of the figure show the transmission coefficients τ_i for the electronic transport through open transport channels i. With increasing distance between the electrodes during the stretching of the wire, less atoms contribute to the transport due to the lateral contraction at the emerging constriction. Finally the entire current flows through single atoms, before the wire breaks at further stretching. In the upper part of the figure, the sum of the channel transmissions are shown as total conductance $G = G_0 \sum_i \tau_i$ (full line), as well as the thermal conductance κ (symbols). The "quantised steps" in the lines result by a successive closing of open transport channels during the wire stretching due to atomic reordering. The values at the vertical line result for the atomic configurations on the right part of the figure.

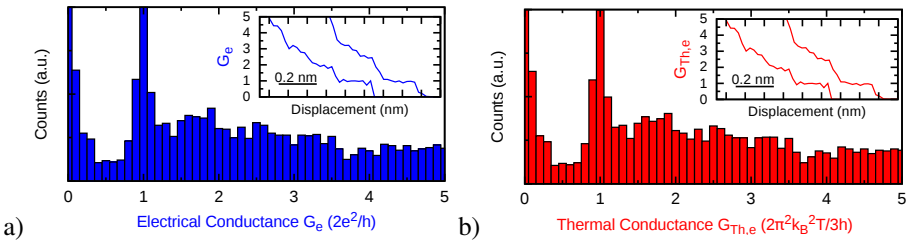

Figure 2. Histograms of the electric (a) and thermal-electronic (b) conductance after averaging over 100 MD simulations (Au, room temperature)[2]. Insets show representative electric and thermal conductance evolutions from these simulations.

important[2] (with M. Matt, J. C. Klöckner, F. Pauly and J. C. Cuevas). The heat transport in atomic nano wires has contributions from atomic motions as well as from electronic motions, both components have to be computed quantum mechanically. By our studies, it became possible to probe the Wiedemann-Franz law, which neglects a contribution from the atomic lattice motion to the heat transport, even on a nanometre length scale. Since this law is an empirical relation, one would perhaps guess, that there is no reason for such a linear relation between the electrical conductance and the heat conductance, since all relevant quantities are quantised. The electrical conductance, for example, is given in units of the conductance quantum, $G_0 = 2e^2/h$, where h is the Planck constant.

Indeed, in a comparison of experimental and theoretical studies[2], it turns out, that the Wiedemann-Franz law has validity for atomic Au- and Pt wires as well. In these studies not only single stretching procedures were analysed (s. Fig. 1), but by extensive ensemble simulations histograms as well (s. Fig. 2), where the correlations provide clear dependencies in the sense of the Wiedemann-Franz law. Whether these insights can be transferred to other materials or deviations from the Wiedemann-Franz law appear, or which other interesting effects affect the transport on atomic length scales, will be investigated in further studies.

Further studies have been done on the orbital origin of the electrical conduction in ferromagnetic atomic-size contacts by comparison of shot noise measurements with our simulations[3].

3 Colloidal Systems

Transport phenomena of colloidal systems in two dimensional channel geometry and a sinusoidal potential have been investigated by Brownian dynamics simulations[4]. Due to the sinusoidal potential, the layering order and the equilibrium structure is disturbed, and as function of the commensurability of the colloidal lattice periodicity and the periodicity of the external potential various modifications of the colloidal mobility result. One example is the appearance of “kinks” and “anti-kinks”, where locally either $n+1$ or $n-1$ particles share n potential minima, when an external constant driving force is applied, and the kinks move in direction of the force and the anti-kinks in the opposite direction. The diffusion can be enhanced by orders of magnitude due to the faster dynamics of the particles at the channel walls.

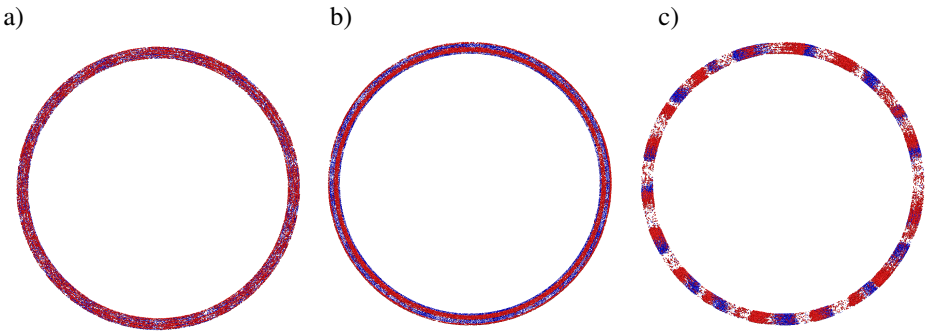

Figure 3. Snapshots of channels with outer radius $R_{max} = 400$ and $\Delta R = R_{max} - R_{min} = 35$ at force a) $F_{max} = 25$, b) $F_{max} = 45$, and c) $F_{max} = 65$.[5] Colours indicate the flow direction of the particles.

In a different study[5] we started to examine a dynamic phase transition in two-dimensional radial ring systems, where half of the particles are driven clockwise and half counterclockwise. The particles interact via a repulsive Yukawa potential, $V(r_{ij}) = U\exp(-\kappa(r_{ij} - \sigma))/r_{ij}$, which also takes a finite particle diameter σ into account, with inverse screening length κ and interaction strength U. To keep a fluid-like behaviour and avoid ordering in equilibrium, a relatively weak potential of $U = 5$ and inverse screening length of $\kappa = 2$ is used at a particle density of $\rho = 0.25$. The two particle types were driven against each other by a radial force $F = F_{max}(R/R_{max})$, acting on each particle in such a way, that the particles move with a constant angular velocity.

The particles often separate in an inner ring and an outer ring. It seems that for large systems (i.e. $R_{max} = 400$) and large forces the particles separate in a different manner. Fig. 3 shows that for small driving forces $F_{max} = 25$ a laning starts on a local scale. At $F_{max} = 45$ the particle separate in four rings, which are not stable over time. For a large force of $F = 65$ an unexpected transition into a clustered state appears. Multiple clusters of one particle type form, which frequently encounter clusters of the other particle type. Between the encounters the particles can move freely, without approaching particles of the other type.

This type of dynamic phase transition only occurs in very large ring systems with outer radius $R_{max} \geq 300$. Yet it is not clear under which conditions this transition occurs. Therefore we need to vary the width of the ring channel ΔR and the interaction strength U between the particles. Additionally we want to proceed to even larger systems with particle numbers between 10000 and 100000. We also plan to investigate whether this kind of transition also occurs even in very large three dimensional systems.

In a masters thesis[6] we investigated binary mixtures of spherocylinders and spheres (s. Fig. 4). A method to recognise clusters was developed and implemented. The mixtures are initialised in a three-dimensional simulation box, which has either periodic boundary conditions or is impenetrable for colloids. The mixtures investigated were then sedimented on the two-dimensional surface of the box by adding a constant external force in z-direction. This process is similar to the experimental setup[7], where a suspension is set up and sedimented to the surface of the liquid by different methods.

Theoretical approaches to the evolution of cluster size as function of colloid density

a) 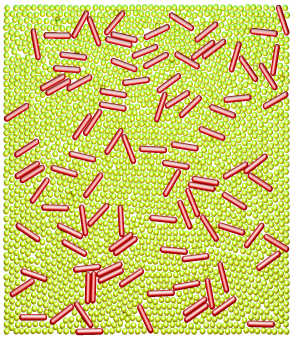 b) 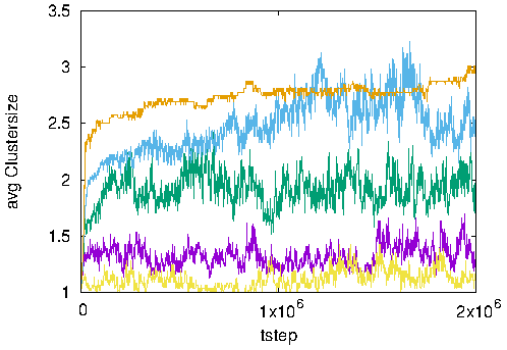

Figure 4. a) Snapshot of a rod-sphere mixture and b) time evolution of the average cluster size of rod particles for different densities of spherical particles[6].

has been made in consistency with the simulation results. Also a method to implement partial charges on the colloids has been programmed. Simulations of different systems of one or two sorts of colloids have been performed which showed a richer phase behaviour, in accordance with the expectations. All the implemented methods unveiled better insight into the structure formation and on options to generate them more easily and keeping them more stable.

4 Nucleation Phenomena and Crystal Growth

Description of nucleation and crystal growth phenomena of real materials is an ongoing topic in science. The development of accurate forcefields for materials like calcium carbonate in water[11], that show nonclassical nucleation behaviour in their growth scenarios, is essential to deliver insights into microscopic effects like ion association by entropy[9], amorphous pre-clusters[12], interaction of crystalline nanoparticles with the solvent[8] and even growth of early stages of nano particles[10]. Regarding one growth process from the ionic solution to the nanoscale crystal, the formation from the association of ions to the amorphous pre-clusters is still a missing piece.

We therefore use a lattice gas model in our canonical Monte-Carlo algorithm with one spin per particle for the type of the particle and another spin for the orientation, to look for the existence of an effect, which is between an ion-chain like growth and the nucleated particle. The model shall capture an ionic solution of crystal particles, each carrying a simple positive or negative charge (like Ca^{2+} and CO_3^{2-}), in a solvent with dipole moments at each particle (like water). The dipole particles get an additional spin value annotating their directional alignment. Putting those particles in a three dimensional square lattice and giving each dipole six orientations, the interaction energies of next neighbours can be directly calculated via charges and orientation of the solvent. The chosen parameters are illustrated in Tab. 1. The displayed relative alignments of next neighbours can be generalised to the three dimensional lattice. Given these Energies H, we run Metropolis Monte-Carlo simulations with two kinds of spin-flips that are applied with equal probability. The first spin flip is the change of the material type at random lattice site and the second spin flip

Particle i	Particle j	Energy H $[k_BT]$	Particle i	Particle j	Energy H $[k_BT]$
$+$	$+$	$+2$	$-$	$\uparrow / \downarrow$	0
$+$	$-$	-2	$\uparrow$	$\uparrow$	+2
$+$	$\rightarrow$	-1	$\uparrow$	$\downarrow$	-2
$+$	$\leftarrow$	$+1$	$\uparrow / \downarrow$	$\leftarrow / \rightarrow$	0
$+$	$\uparrow / \downarrow$	0	$\rightarrow$	$\rightarrow$	-1
$-$	$-$	$+2$	$\leftarrow$	$\rightarrow$	+1
$-$	$\rightarrow$	$+1$	$\rightarrow$	$\leftarrow$	+1
$-$	$\leftarrow$	-1			

Table 1. Illustration of next neighbour $< ij >$ interaction energies. $+$ and $-$ are positive and negative charged ions, $\uparrow$ is the dipol particle of the solute with opposite charges at each end. The head of the arrow is the positive charge.

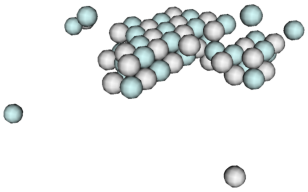

Figure 5. Typical configuration of the solutes in the lattice gas. The two colours show the different charge of the solute particles.

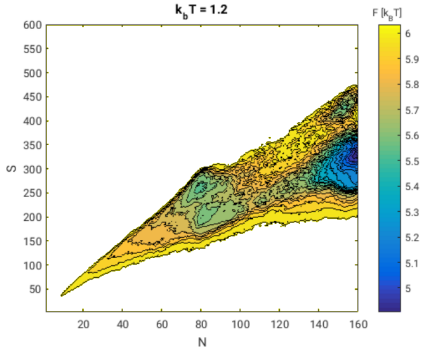

Figure 6. Free energy of the largest cluster in the system in dependence of the cluster size N and the cluster surface S for $k_BT = 1.2$.

is the change of the orientation of a randomly chosen dipole. As described in Ref. 13, a constant density of the solute is established by requiring after each spin-flip that the number of solutes N_i of type $i = 1, 2$ is in the interval $[N_{dens}, N_{dens} + 1]$, where N_{dens} is the number of solutes given by the desired density. This way the lattice gas is simulated in the canonical ensemble because errors by the small density fluctuation vanish quickly ($\propto 1/L^d$) with system size L in d dimensions. During runtime, the free energy of various reaction coordinates is estimated via the metadynamics protocol[14]. In Fig. 5 a typical configuration of the solutes is shown for a temperature at $k_BT = 1.2$. Due to the influence of the dipoles in the solvent the clusters exhibit large surfaces. In Fig. 6 the free energy of the formation of the largest cluster is shown for the reaction coordinates N (cluster size) and S (cluster surface). For cluster sizes smaller than $N = 60$ the free energy forces the clusters to exhibit the largest possible surface, e.g. to grow as a chain, gaining energy by growth. This matches to the entropic force driving ion association via hydration shells in Ref. 9. At a Cluster Size of $N \approx 80$ further growth as a chain is suppressed and via a small energy barrier the chains collapse to clusters with roughly the same amount of particles, but with

lower surfaces. Those plate like clusters can then grow in size via a second energy barrier, which maximum is at $N \approx 110$.

5 Hydrodynamics Simulations

Applying the smoothed particle hydrodynamics (SPH) method (a comprehensive review of the method is given in Ref. 15) to mesoscopic system sizes is an aim of our NIC project. In this context progress has been made in the context of spinodal decomposition of liquid-vapour systems. We already successfully applied the massively parallelised SPH code GADGET2[16] to liquid-vapour spinodal decomposing van der Waals fluids (vdW-SPH)[17], where a scaling thermostat was introduced, such that latent heating is fully suppressed and keeps the mean temperature constant.

In the last granting period, we further investigated the influence of the strength of heat bath coupling on the demixing behaviour in spinodal decomposing one component liquid-vapour systems. The vdW-SPH method is used for the simulation. A newly developed thermostat for SPH is introduced that is based on the Berendsen thermostat, which is a common thermostat in molecular dynamics. It controls the strength of heat bath coupling and allows for quenches with exponential temperature decay at a certain thermalisation time scale. The present method allows us to bridge several orders of magnitude in the thermalisation time scale. The early stage, as shown in Fig. 7, is highly affected by the choice of time scale. A transition from exponential growth to a $1/2$ ordinary power law scaling in the characteristic lengths ξ_l is observed. At high initial temperatures the growth is logarithmic. The comparison with pure thermal simulations reveals latent heat to raise the mean system temperature. Large thermalisation time scales and thermal conductivity are figured out to affect a stagnation of heating, which is explained with convective processes. Furthermore, large thermalisation time scales are responsible for a stagnation of growth of domains, which is temporally embedded between early and late stage of phase separation. Therefore, it is considered as an intermediate stage. We observed an aspect concerning

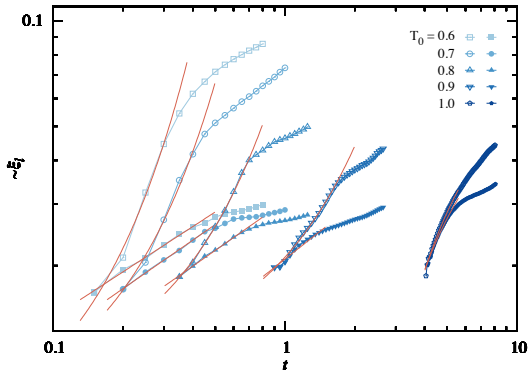

Figure 7. The early and, if apparent, the intermediate stages of ξ_l for time scales $\tau = 10^{-4}$ (open symbols) and 10^1 (filled symbols) for different quench depths at $T_0 = 0.6$, 0.7, 0.8, 0.9, and 1.0. Overlaying curves (red) belong to least square fits with the parameters.

this stage, namely that choosing larger thermalisation time scales increases the duration. Moreover, it is observed that diffuse interfaces are formed during this stage, provided that the stage is apparent, which depends on the thermalisation time scale.

We showed that the differences in the evolution between pure thermal simulations and simulations with an instantaneously scaled mean temperature[17] can be explained by the thermalisation process, since a variation of the time scale allows for the bridging between these cases of limit[18].

For our simulations of the gas dynamics and their interplay with magnetic fields in galaxies we use the development version of GADGET[16], GADGET-3. In order to investigate magnetic fields the smoothed particle magnetohydrodynamics (SPMHD) implementation of Ref. 19 is used in a study that focused on magnetic driven outflows in disk galaxies[22]. In another study[20] we investigated the small scale magnetic field of our own Galaxy, the Milky Way. Therefore, we use the HAMMURABI code[21] to compute simulated mock observations. We present a new prescription for the small scale field that reveals important knowledge of the characteristics of random magnetic field fluctuations and complements existing models for the total Galactic magnetic field.

Acknowledgements

Discussions and collaborations are gratefully acknowledged to J. C. Cuevas, F. Pauly, J. C. Klöckner, L. Cui, W. Jeong, S. Hur, E. Meyhofer, and P. Reddy on the electronic and thermal transport studies, to K. Dolag, A. M. Beck, R. Beck, and A. W. Strong on magneto-hydrodynamics simulations, and to C. Peter on nucleation studies. We thank the NIC for computer time on JURECA for the project HMZ07 and the SFBs 1214 and 767 for support.

References

1. M. Dreher, F. Pauly, J. Heurich, J. C. Cuevas, E. Scheer, P. Nielaba, Phys. Rev. **B 72**, 075435, 2005.
2. L. Cui, W. Jeong, S. Hur, M. Matt, J. C. Klckner, F. Pauly, P. Nielaba, J. C. Cuevas, E. Meyhofer, P. Reddy, Science **355**, 1192, 2017.
3. R. Vardimon, M. Matt, P. Nielaba, J. C. Cuevas, O. Tal, Phys. Rev. **B 93**, 085439, 2016.
4. U. Siems, P. Nielaba, Phys. Rev. **E 91**, 022313, 2015.
5. T. Vater, Bachelor Thesis, University of Konstanz, 2016.
6. S. Haun, Master Thesis, University of Konstanz, 2017.
7. A. Ulman, Chemical Reviews **96**, 1533, 1996.
8. D. J. Cooke and J. A. Elliot, J. Chem. Phys. **127**, 104706, 2016.
9. M. Kellermeier, P. Raiteri, J. K. Berg, A. Kempter, J. D. Gale, Chem. Phys. Chem. **17**, 1, 2016.
10. G. A. Tribello, F. Bruneval, C. Liew, M. Parrinello, J. Phys. Chem. B **113**, 11680, 2009.
11. P. Raiteri, J. D. Gale, D. Quigley, P. Rodger, J. Phys. Chem. C **114**, 5997, 2010.
12. P. Raiteri and J. D. Gale, J. Am. Chem. Soc. **132** (49), 17623, 2010.
13. F. Schmitz, P. Virnau, K. Binder, Phys. Rev. E **87**, 053302, 2013.

14. A. Laio, M. Parrinello, Proc. Natl. Acad. Sci. U S A, **99** (20), 12562–12566, 2002.
15. D. J. Price, J. Comput. Phys. **3**, 759, 2012.
16. V. Springel, MNRAS **4**, 1105, 2005.
17. M. Pütz, P. Nielaba, Phys. Rev. **E91**, 032303, 2015.
18. M. Pütz, P. Nielaba, Phys. Rev. **E 94**, 022616, 2016.
19. K. Dolag, F. Stasyszyn, MNRAS **398**, 1678, 2009.
20. M. C. Beck, A. M. Beck, R. Beck, K. Dolag, A. W. Strong, P. Nielaba, JCAP **05**, 056, 2016.
21. A. Waelkens, T. Jaffe, M. Reinecke, F. S. Kitaura, T. A. Enßlin, A&A, **495**, 697, 2009.
22. U. Steinwandel, Master Thesis, University of Konstanz, 2017.